The Effect of Iron Content on the Iron-Containing Intermetallic Phases in a Cast 6060 Aluminum Alloy

L. SWEET, S.M. ZHU, S.X. GAO, J.A. TAYLOR, and M.A. EASTON

The effect of iron content, ranging from 0.1 to 0.5 wt pct, on the formation of Fe-containing intermetallic phases in a cast 6060 aluminum alloy was investigated. Various characterization techniques, including optical microscopy, scanning electron microscopy (SEM), electron backscatter diffraction (EBSD), and transmission electron microscopy (TEM) were used to examine the identity, morphology, and prevalence of the Fe-Al and Fe-Al-Si intermetallic phases. The predominant phase is found to be β-Al_5FeSi at lower Fe levels, but this is replaced by α-AlFeSi (bcc structure) with increasing Fe content. The Fe containing intermetallic phases observed are compared to those predicted using the Scheil module of THERMO-CALC software, and the similarities and discrepancies are discussed.

DOI: 10.1007/s11661-010-0595-6

I. INTRODUCTION

ONE of the challenges for the sustainability of the aluminum industry is the increased use of recycled material for the production of wrought Al-based alloys. While Al-based alloys are often regarded as being 100 pct recyclable, there are some important factors that need to be taken into consideration when recycling. One of these is the impact of increasing Fe level.[1] Increased Fe levels can be tolerated, and even appreciated in high pressure die casting alloys, as they can reduce die sticking, although the resultant phases can contribute to porosity formation in some foundry alloys.[2,3] In wrought alloys, some Fe can also be beneficial in restricting grain growth during homogenization,[4] but these alloys are much less tolerant to increasing Fe content as the brittle intermetallic particles formed with increased Fe contents can reduce the ductility and formability of these alloys.[5,6] Increased Fe levels may also affect the hot tearing susceptibility of Al-based alloys.[7] Hence, there is a need to understand how changing Fe content affects the formation of Fe-containing intermetallic phases in Al alloys.

The metallurgy of the Fe-containing intermetallics in Al alloys is complicated, because there are so many different phases that can form. There have been several critical reviews on these topics since the 1980s,[8–10] mainly focused on Al-Si casting alloys.

In the simple Al-Fe binary system, the most common Al-rich intermetallic phase has been given two different stoichiometries,[11] Al_3Fe[12] and $Al_{13}Fe_4$,[13] with a monoclinic crystal structure ($a = 1.549$ nm, $b = 0.808$ nm, $c = 1.248$ nm, $\beta = 107.72$ deg). The binary system exhibits a eutectic composition of approximately 1.8 wt pct Fe and a eutectic temperature of 928 K (655 °C).[12]

When Si is present, as in the case of 1xxx, 3xxx, or 6xxx series alloys, a number of other phases may form, depending upon the relative contents of each element.[14,15] The two most common phases found in Al-Fe-Si ternary alloys are usually denoted as β-Al_5FeSi (monoclinic: $a = b = 0.612$ nm, $c = 4.15$ nm, $\beta = 91$ deg[12] or $a = b = 0.618$ nm, $c = 2.08$ nm, $\beta = 91$ deg[16]) and α-Al_8Fe_2Si (hexagonal: $a = 1.23$ nm, $c = 2.63$ nm[12]),[17] though other stoichiometries have been used by other authors, *e.g.*, Rivlin *et al.*[15]

β-Al_5FeSi tends to form at lower Fe contents than does α-Al_8Fe_2Si. At even higher Fe contents, Al_3Fe can form. However, while the level of Fe indicates which phase will precipitate directly from the melt upon solidification, there are a series of complicating peritectic reactions that may also occur as the temperature decreases; *i.e.*,

$$L + Al_3Fe \rightarrow \alpha - Al_8Fe_2Si \qquad [1a]$$

$$L + \alpha - Al_8Fe_2Si \rightarrow \beta - Al_5FeSi \qquad [1b]$$

There are reports in the literature of the simultaneous occurrence of both of these reactions[11,18] and of the former reaction occurring preferentially, followed by the latter reaction in 6xxx series alloys.[13,19] Manganese-containing alloys follow a similar path where the Mn-containing form of α-AlFeMnSi is involved.[20] While this would suggest that β-Al_5FeSi should be the equilibrium Fe-containing phase present at lower temperatures, it is known that peritectic reactions rarely go to completion.[11,13] In fact, it has been considered that there is a peritectic reaction, which initiates on the surface of the previous substrate, followed by a peritectic transformation, which is limited by solid-state

L. SWEET, Senior Research Engineer, S.M. ZHU and S.X. GAO, Research Fellows, and M.A. EASTON, Program Manager, are with CAST Co-operative Research Centre (CAST CRC), Department of Materials Engineering, Monash University, Victoria 3800, Australia. Contact e-mail: lisa.sweet@monash.edu J.A. TAYLOR, Principal Research Fellow, is with CAST Co-operative Research Centre (CAST CRC), School of Mechanical and Mining Engineering, The University of Queensland, St Lucia, Queensland 4072, Australia.

Manuscript submitted July 4, 2010.
Article published online January 8, 2011

diffusion. Hence, it is likely that this kinetic process controls the final phase formation rather than the thermodynamics of the system.

Al_3Fe, α-Al_8Fe_2Si, and β-Al_5FeSi phases have different characteristic morphologies. It has been reported that both Al_3Fe and β-Al_5FeSi are faceted phases,[14] while the α-Al_8Fe_2Si exhibits a Chinese-script morphology. Hence, simple optical metallography can give an indication of which phases are probably present, especially if etchants are used to distinguish the intermetallic phases by color. However, since the volume fraction of intermetallics tends to be quite small in lean 6xxx series alloys, it can be difficult to conclusively identify the intermetallics in this way; *e.g.*, Chinese-script such as α-Al_8Fe_2Si lying along a grain boundary may appear to be a faceted phase. This can present even more of a problem in heat-treated samples, where phase transformations may occur while the morphology of the parent phase is retained.

In addition to the aforementioned three phases (*i.e.*, Al_3Fe, α-Al_8Fe_2Si, and β-Al_5FeSi) commonly observed in the Al-Fe-Si system, there are some other ternary phases that have also been reported, *e.g.*, Al_4FeSi_2 (tetragonal: $a = 0.612$ nm, $c = 0.948$ nm)[21] and Al_3FeSi (C-centered monoclinic: $a = 1.78$ nm, $b = 1.025$ nm, $c = 0.890$ nm, $\alpha = 132$ deg).[12]

It is generally accepted, as noted previously, that in the ternary Al-Fe-Si system, a hexagonal ternary phase α-Al_8Fe_2Si can form. However, with the presence of small amounts of transition metals, *e.g.*, V, Cr, Mo, W, Mn, and Cu,[22] an alternative body-centered-cubic phase forms. In the presence of Mn, this phase has been designated as $Al_{19}Fe_4MnSi_2$[23,24] but is more often designated as $Al_{15}(Fe,Mn)_3Si_2$ or $Al_{12}(Fe,Mn)_3Si$. While these are also designated α phase and also generally have a Chinese-script morphology,[17,18] they are found to have a different crystal structure (bcc: $a = 1.256$ nm)[12,17,25] and stoichiometry to the hexagonal α-Al_8Fe_2Si phase.

The Mn is commonly added to 6xxx series alloys to restrict the formation of β-Al_5FeSi platelets (needles in two-dimensional (2-D) cross section) and instead promote the less faceted and more refined α_c-Al(Fe,Mn)Si phase, because this is believed to improve the formability and surface finish of extrusions.[26] It has been claimed that the cubic α phase cannot be present in the ternary Al-Fe-Si system;[27] however, there are examples where the cubic form has been found in the as-cast microstructure in an essentially Mn-free alloy.[18,28] In this article, the two α phases (cubic and hexagonal) will be denoted from now on according to their crystallography, α_c and α_h, respectively. However, the subscript is sometimes dropped when the crystal structure is not being specified, *e.g.*, for a phase with a Chinese-script morphology observed optically.

The addition of Mg in 6xxx series alloy has a relatively minor effect on the Fe-containing phases in the microstructure; *e.g.*, it does not affect the type of α-AlFeSi.[27] However, two new phases can form: π-$Al_8FeMg_3Si_6$ (hexagonal: $a = 0.663$ nm, $c = 0.794$ nm) and Mg_2Si (cubic: $a = 0.635$ nm).[17,29,30] Both phases form at lower temperatures than β-Al_5FeSi and are typically present in minor amounts after solidification. These phases can display a Chinese-script morphology,[30] although after etching, they may exhibit different colors than the α-AlFeSi phases.

This article investigates the effect of Fe content on the formation of Fe-containing intermetallic phases in a cast 6060 Al alloy. A variety of microstructural characterization techniques including optical microscopy, scanning electron microscopy (SEM), energy dispersive X-ray spectroscopy (EDX), electron backscatter diffraction (EBSD), and transmission electron microscopy (TEM) were used to determine the identity and distribution of the dominant intermetallic phases.

II. EXPERIMENTAL METHODS

A series of alloys were cast with Si and Mg contents within the AA6060 alloy specification (0.52 to 54 wt pct Si and 0.35 to 0.40 wt pct Mg), but varying in Fe content (0.1 to 0.5 wt pct). The alloys were grain refined using Al5Ti1B grain refiner additions at 0.05 pct Ti to produce samples with as-cast grain size similar to that found in direct chill (DC) cast alloys.[31] The detailed compositions of these alloys are shown in Table I. Unless otherwise specified, all compositions are expressed in weight percentage (wt pct). The alloys were cast into bars (180-mm long, 24-mm deep, and 20-mm wide) in a preheated steel mold. The mold was designed to simulate cooling rates common to DC casting, *i.e.*, approximately 2 K/s.[32] Samples for metallography were taken from the central region of the alloy bars. Specimens were prepared for optical microscopy, SEM, and TEM to observe the structure at three different scales, and to obtain information on both phase morphology and phase constitution.

Samples for optical microscopy were polished according to normal metallographic techniques, etched with 0.5 pct HF and then viewed using standard optical microscopy techniques. Differentiation and identification of phases is typically based on their distribution, morphology, and color (etched and unetched). However, there are limitations to this as different phases may have similar morphologies and spatial growth restrictions can have as much influence on the morphology as can phase identity and preferred growth mode.

To further reveal the morphology and interconnectedness in three dimensions of intermetallic phases, some samples were deeply etched to preferentially remove the matrix phase. Deep etching was carried out on alloy

Table I. Compositions of the 6060 Alloy Samples as Determined by Optical Emission Spectroscopy; the Alloys are Designated by the Nominal Fe Content

	Elemental Composition (Weight Percent)					
Alloy	Si	Mg	Fe	Mn	Ti	Al
0.1 Fe	0.52	0.35	0.09	≤0.001	0.05	bal
0.2 Fe	0.56	0.40	0.20	≤0.001	0.05	bal
0.3 Fe	0.53	0.39	0.28	≤0.001	0.05	bal
0.5 Fe	0.52	0.35	0.50	≤0.001	0.05	bal

samples that were ground to a 1200 grit SiC finish and then were held face down in a gently stirred solution of iodine in methanol (10 g in 100 mL) at room temperature for approximately 4 hours (variable time depending on particular alloy sample). The samples were then rinsed gently in methanol and air dried prior to examination by SEM. The technique is described[33] as being suitable for identifying Al(Fe,Si) and Al(Mn,Si) phase types.

Scanning electron microscopes equipped with EDX and EBSD can provide both chemical and crystallographic information about phases as well as detailed structure, at a scale where phases are more readily recognized. For this work, samples with dimensions 10 mm × 8 mm × 1 mm were cut from the alloy bars. After mechanical polishing, the samples were prepared with 0.05-μm colloidal silica suspension for 10 minutes and 0.05-μm alumina suspension for 2 minutes. The samples were examined using a JEOL* JSM 7001F field emission scanning electron microscope, equipped with an HKL Channel 5 (Oxford Instruments plc., Oxfordshire, United Kingdom) EBSD system and a Bruker Quantax (Bruker AXS Inc., Madison, WI) EDX system. EDX is used to identify different phases by comparing the ratio of iron to silicon or manganese to "known" ratios within the intermetallic phases.[34,35] However, since there is some disagreement with regard to the exact ratios, critical analysis of results is required.

TEM is useful to identify the crystal structure of various phases with a high degree of precision using diffraction patterns coupled with EDX. However, it can be difficult to ensure each phase is represented in a thin foil specimen, and it is also difficult to correlate phases found in TEM with those observed at the coarser microstructure scale. Samples for TEM observation were sliced into sheets 0.6-mm thick. Discs 3 mm in diameter were punched from the alloy sheets, ground to a thickness of 0.15 mm, and then twin-jet electrochemically polished in an electrolyte of 33 pct nitric acid in methanol at 248 K (–25 °C) and 0.1 A.

Some foils were further ion milled at low angles using a Gatan Precision Ion Polishing System. Characterization of microstructures was performed in a PHILIPS** CM20 TEM instrument, equipped with an Oxford Instruments (Oxfordshire, United Kingdom) standardless EDX, operating at 200 kV. Microdiffraction was performed in conventional TEM mode using a 30-mm condenser aperture and an electron probe nominally 15 nm in diameter.

*JEOL is a trademark of Japan Electron Optics Ltd., Tokyo.

**PHILIPS is a trademark of Philips Electronic Instruments Corp., Mahwah, NJ.

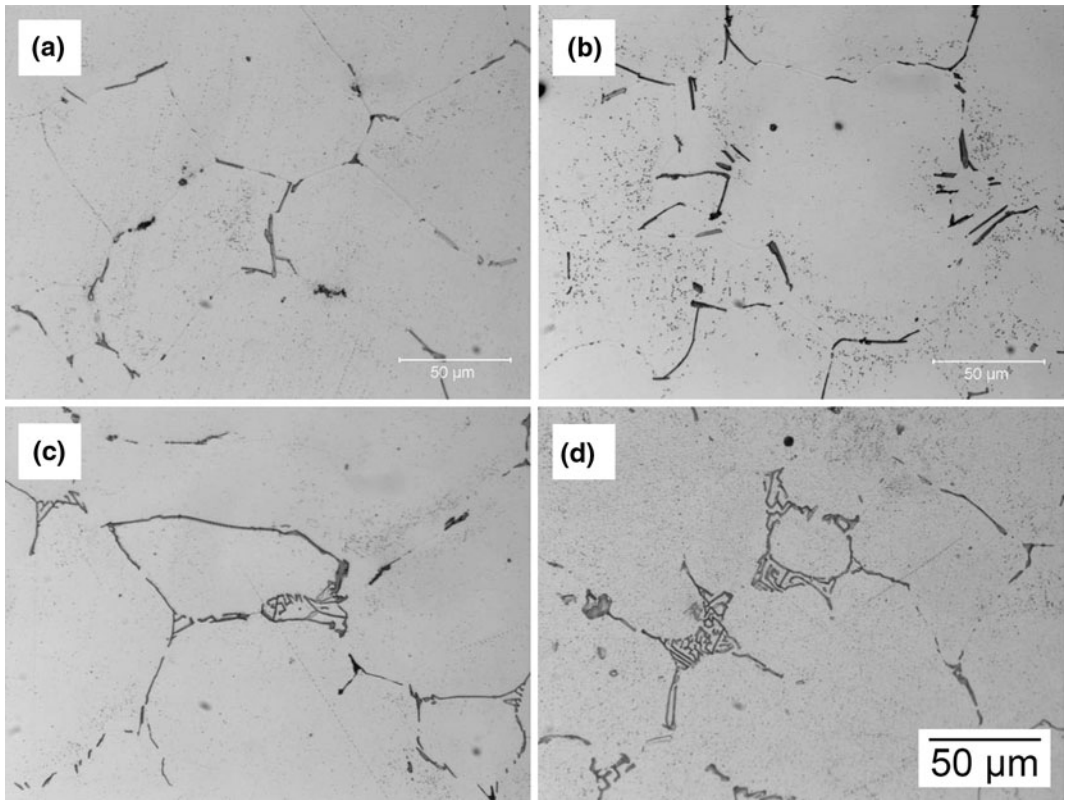

Fig. 1—Optical micrographs showing the typical morphology of intermetallic particles in the 6060 alloys containing (*a*) 0.1, (*b*) 0.2, (*c*) 0.3, and (*d*) 0.5 wt pct Fe. Note the morphological evolution of the particles from the predominantly faceted feature to the Chinese-script appearance with increasing Fe content. All micrographs are shown at the same scale.

THERMO-CALC[†] (TCW4) software with database

[†]THERMO-CALC is a trademark of Thermo-Calc Software, Stockholm, Sweden.

TTAL4 was used to predict phases present in the 6060 alloys with differing Fe contents, using the Scheil module. The Scheil (or Gulliver–Scheil[36]) equation is typically used to predict solidification paths in alloys using the assumptions that there is no diffusion in the solid and instantaneous diffusion in the liquid. The great advantage of this equation is that good estimations of solidification paths can be obtained without the use of diffusion data and complex solidification models. While some backdiffusion occurs, including in Al-Si-Mg alloys,[29] such deviations are not great. A recent comparison between a computational solidification model and the Gulliver–Scheil equation for an Al-Si alloy showed that slower solidification rates, in their case 0.1 K/s, gave excellent correlation.[37] The solidification rates here are approximately 2 K/s, so it appears that it is a reasonable assumption to use the Gulliver–Scheil equation. A comparison was then made between the experimentally observed phases and those predicted by THERMO-CALC.

III. OBSERVATIONS AND RESULTS

A. *Observations by Optical Microscopy*

Figure 1 shows typical microstructures of 6060 alloys with Fe content varying from 0.1 to 0.5 wt pct. The amount of intermetallic particles appears to increase with increasing Fe content. The intermetallics are located predominantly at the grain boundaries, both along and across them. At the low Fe contents (0.1 to 0.2 wt pct), the intermetallic particles appear to be quite faceted with a needlelike morphology seen in cross-sectional view (Figures 1(a) and (b)). At medium Fe content (0.3 wt pct), some particles with Chinese-script morphology are observed, although most of the intermetallic particles still seem to be needlelike (Figure 1(c)). At the highest Fe content (0.5 wt pct), a large portion of the intermetallic particles display the Chinese-script morphology (Figure 1(d)). As will be shown later in this article, the faceted and Chinese-script particles were indentified to be β-Al_5FeSi phase and α_c-AlFeSi phase, respectively.

B. *Observations by SEM*

While optical microscopy allowed observation of the different morphologies of the β-Al_5FeSi and α_c-AlFeSi

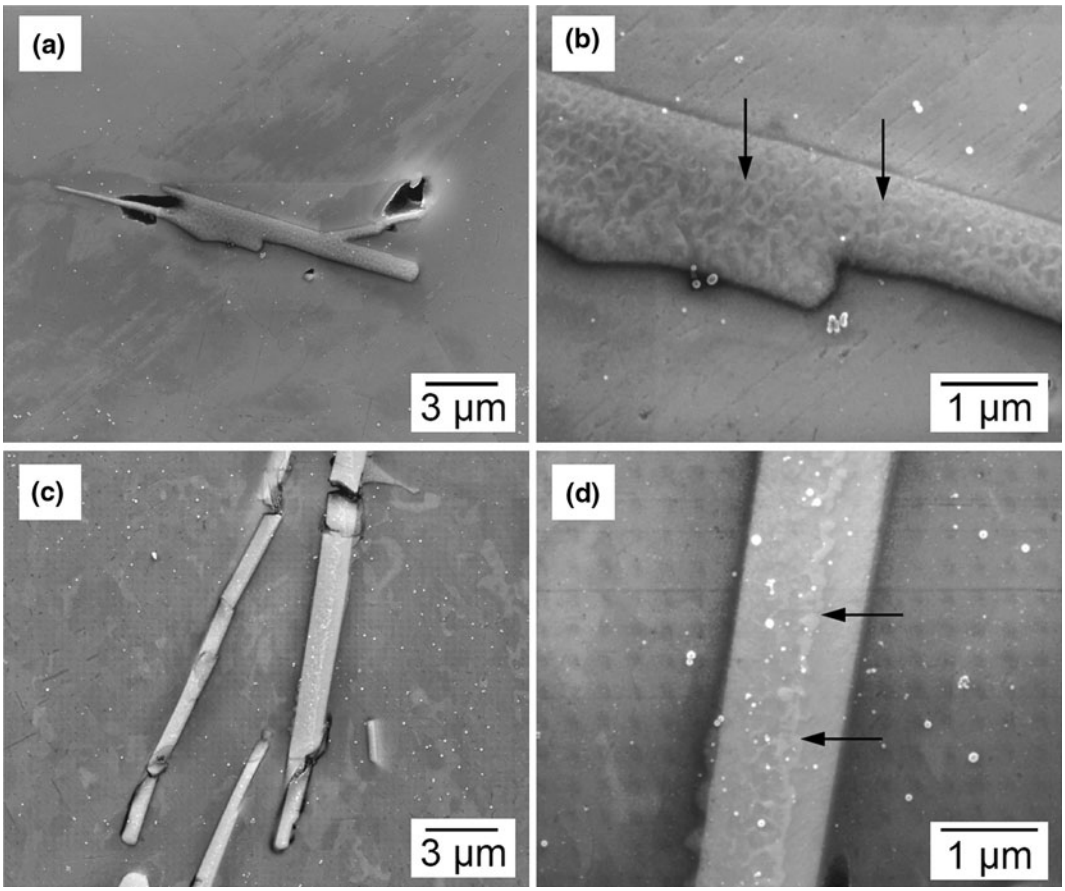

Fig. 2—SEM SEIs of the faceted intermetallic phase in the 6060 alloys containing (*a*) and (*b*) 0.1 wt pct Fe and (*c*) and (*d*) 0.3 wt pct Fe. At high magnification, a lacy feature (arrowed) is revealed. White spots are a polishing artifact.

phases, SEM microscopy was able to reveal different features on the polished cross sections of these phases. Figures 2 and 3 show the SEM images of the β-Al_5FeSi and α_c-AlFeSi phases in these alloys, respectively. In Figure 2, the faceted morphology of the β-Al_5FeSi phase can be clearly seen at low magnification (Figures 2(a) and (c)). At high magnification, the β-Al_5FeSi phase appears to display a lacy feature on the surface (Figures 2(b) and (d)). For the Chinese-script α_c-AlFeSi phase, the surface is always less ornate or fairly featureless, even at high magnification (Figures 3(b) and (d)). Noting that the lacy feature on the surface of the β-Al_5FeSi phase was usually observed when the sample was polished with colloidal silica for a slightly longer time, we ascribe the features observed on the surface of these phases to the etching effect of colloidal silica, though the effect is very weak. The reason why β-Al_5FeSi and α_c-AlFeSi phases exhibited different etching responses is not clear at this moment. Nevertheless, the observed different features on these phases can be used as a rough indication of the phase identity.

It is also noted from the SEM images that shrinkage voids tend to form around intermetallic phases, and some intermetallic particles show cracking. However, there appears to be no obvious difference between the β-Al_5FeSi and α_c-AlFeSi phases in these aspects.

C. *Observations of Deep Etched Samples*

Figure 4 shows SEM observations of the deep etched samples with different Fe levels. It can be seen that there is a strong interconnectedness between intermetallic particles. Even at 0.1 wt pct Fe, the intermetallic particles have already developed a three-dimensional (3-D) network along the grain boundaries. However, at this Fe level, it was not fully connected and therefore some intermetallic particles tended to dislodge and fall into the etchant during deep etching. With increasing Fe content, the intermetallic network became denser and more continuous and therefore less prone to this effect.

Figure 5 shows higher magnification images of the deep etched 0.1 wt pct Fe and 0.5 wt pct Fe samples, where the dominant intermetallic phase is β-Al_5FeSi and α_c-AlFeSi, respectively. The 3-D morphology of the intermetallic phases is more obvious. The more faceted angular shape of the β-Al_5FeSi particles in the 0.1 wt pct Fe alloy is in contrast to the α_c-AlFeSi phase in the 0.5 wt pct Fe alloy, which after deep etching shows a morphology resembling seaweed, rather than Chinese-script, as it is traditionally described in cross-sectional views.

D. *EBSD and EDX Analysis*

In the 0.1 wt pct Fe alloy, β-Al_5FeSi was identified to be the major intermetallic phase. Typical SEM secondary electron image (SEI), EBSD pattern, and

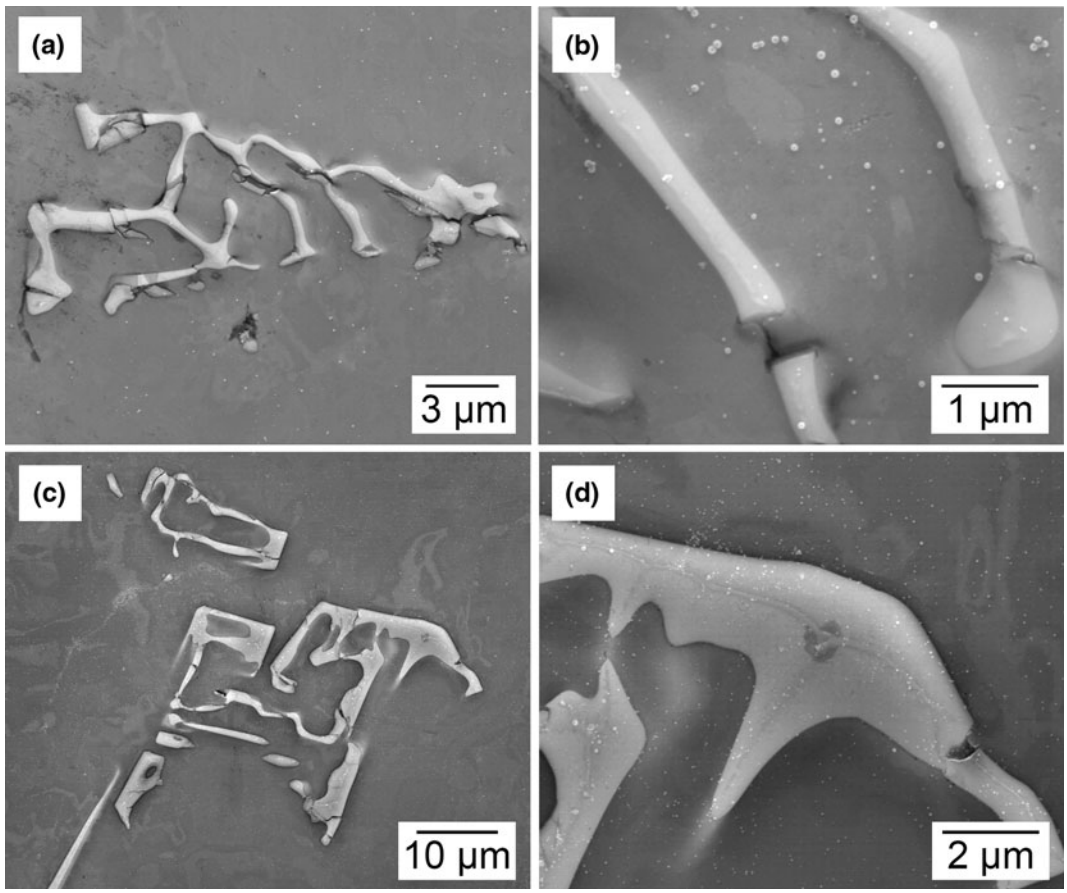

Fig. 3—SEM SEIs of the Chinese-script intermetallic phase in the 6060 alloys containing (*a*) and (*b*) 0.3 wt pct Fe and (*c*) and (*d*) 0.5 wt pct Fe. At high magnification, the particles are quite featureless. White spots are a polishing artifact.

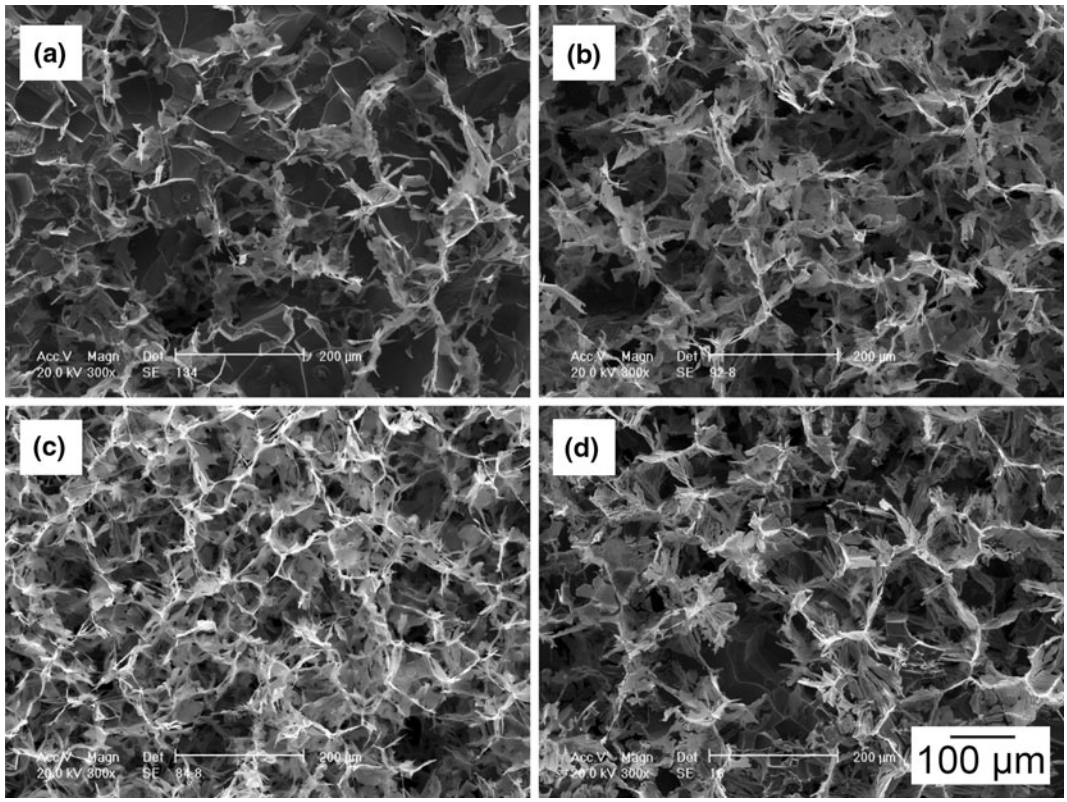

Fig. 4—SEM secondary electron micrographs showing the interconnectedness of the intermetallic particle networks in deep etched 6060 alloy samples containing (*a*) 0.1, (*b*) 0.2, (*c*) 0.3, and (*d*) 0.5 wt pct Fe. All images are shown at the same scale.

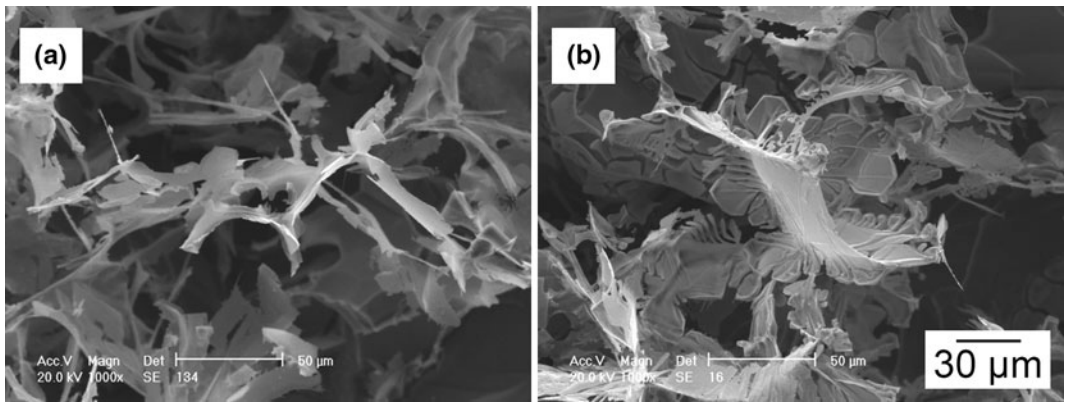

Fig. 5—Deep etched structures at high magnification showing the morphology of (*a*) β-Al_5FeSi intermetallic phase in the alloy containing 0.1 wt pct Fe and (*b*) the Chinese script α_c-AlFeSi intermetallic in the alloy containing 0.5 wt pct Fe.

EDX analyses of the intermetallic phase are shown in Figure 6. The EDX analyses of several particles give a near 1:1 Fe to Si ratio (at. pct) in composition. The EBSD pattern can be well indexed according to a monoclinic crystal structure with $a = 2.081$, $b = 0.618$ nm, $c = 0.616$ nm, and $\beta = 90.42$ deg.[23]

Two types of major intermetallic phase were identified in the 0.2 wt pct Fe alloy using EDX and EBSD: β-Al_5FeSi and α_c-AlFeSi, with the β-Al_5FeSi present in greater amounts. Typical SEM-SEI, EBSD pattern, and EDX analysis of the α_c-AlFeSi particles are shown in Figure 7. The indexing of the EBSD pattern suggests that the α_c-AlFeSi phase has a bcc structure ($a =$ 1.256 nm) matching that of the phase(s) variously designated as $Al_{12}Fe_3Si$, $Al_{15}(Fe,Mn)_3Si_2$, or $Al_{19}Fe_4MnSi_2$. The ratio between Fe and Si in composition (at. pct) obtained from EDX analysis is close to 2, typically 2.1 to 2.2. On this basis, it is closest to the reported $Al_{19}Fe_4MnSi_2$ phase; however, this comparison ignores the Fe substitution that is likely to occur in the absence of Mn in these experimental alloys.[24] In contrast to β-Al_5FeSi, the α_c-AlFeSi particles appear less faceted in appearance and tend to show early script-like characteristics. In addition, a very small amount of the Al_3Fe phase was observed. In the 0.3 wt pct Fe alloy, a higher percentage of α_c-AlFeSi was observed with less β-

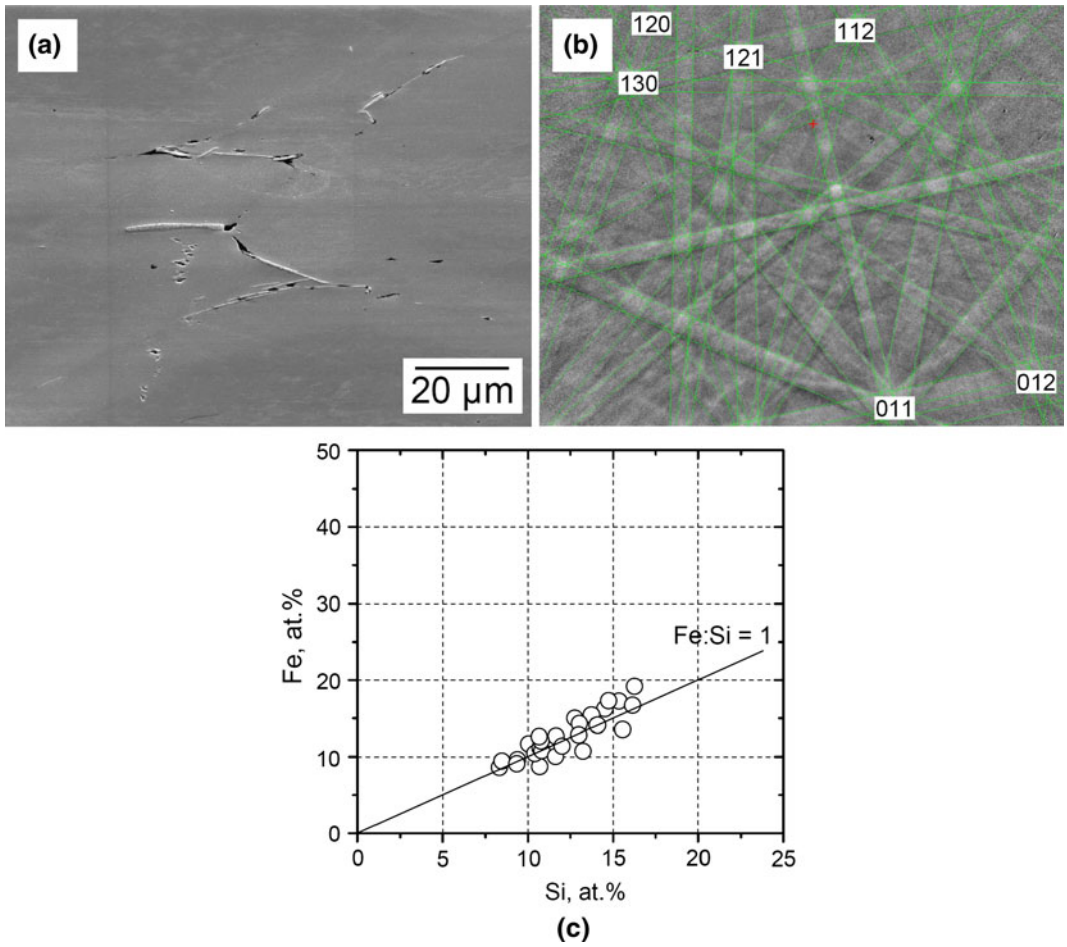

Fig. 6—(*a*) SEM SEI, (*b*) EBSD pattern, and (*c*) EDX analyses of the faceted intermetallic phase observed in the 6060 alloy containing 0.1 wt pct Fe. The EBSD pattern is indexed according to β-Al_5FeSi.

Al_5FeSi present compared with lower Fe contents. In addition, Al_3Fe was occasionally detected. No images are shown for this alloy as they were similar to those of the 0.2 wt pct Fe alloy shown in Figure 7.

In the 0.5 wt pct Fe alloy, the intermetallic phases were identified from the EBSD patterns as being either α_c-AlFeSi as the dominant phase or Al_3Fe as the minor phase. Figure 8 shows an SEM micrograph of a region where both α_c-AlFeSi and Al_3Fe phases are present and the corresponding indexed EBSD patterns. The EBSD pattern for Al_3Fe phase can be well indexed according to a monoclinic crystal structure with lattice parameters $a = 1.549$ nm, $b = 0.808$ nm, $c = 1.248$ nm, and $\beta = 107.72$ deg. The Al_3Fe particles are observed as long platelets extending through the grains.

A summary of the Fe-containing phases indentified by EBSD in each of the alloys is given as follows:

0.1 wt pct Fe: β-Al_5FeSi
0.2 wt pct Fe: β-Al_5FeSi (major) + α_c-AlFeSi (minor)
0.3 wt pct Fe: β-Al_5FeSi + α_c-AlFeSi + Al_3Fe (little)
0.5 wt pct Fe: α_c-AlFeSi (major) + Al_3Fe (minor)

E. *TEM Analysis*

TEM analysis was conducted to confirm the phase identifications by EBSD. For alloys containing 0.1 to 0.3 wt pct Fe, most of the Fe-containing particles were indentified to be β-Al_5FeSi by electron diffraction. Although EBSD suggested the presence of α_c-AlFeSi in the 0.2 wt pct Fe alloy and Al_3Fe in the 0.3 wt pct Fe alloys, these phases were only occasionally observed by TEM due to their occurrence in small amounts. As an example, a TEM image of intermetallic particles and their corresponding diffraction patterns for the 0.3 wt pct Fe alloy are shown in Figure 9. In this case, a β-Al_5FeSi particle appears to be sandwiched, with π-$Al_8FeMg_3Si_6$ phase on either side. This is indicative of a known peritectic reaction.[12] The β-Al_5FeSi particle exhibits a (001) faceted morphology and the presence of planar faults on the (001) planes.

For the 0.5 wt pct Fe alloy, most particles observed by TEM are α_c-AlFeSi, while Al_3Fe particles were rarely spotted. Figure 10 shows an Al_3Fe particle within an α_c-AlFeSi phase. This is indicative of the peritectic reaction described in Eq. [1a], although it may be that α_c-AlFeSi merely nucleates on the surface of the Al_3Fe. EDX analyses of three α_c-AlFeSi particles (Table II) indicate that the ratio between Fe and Si in composition (at. pct) is in the range of 2.1 to 2.2, suggesting that the stoichiometry is neither $Al_{12}Fe_3Si$ nor $Al_{15}(Fe,Mn)_3Si_2$. Electron diffraction patterns recorded from the α_c-AlFeSi particles can be indexed consistently as a

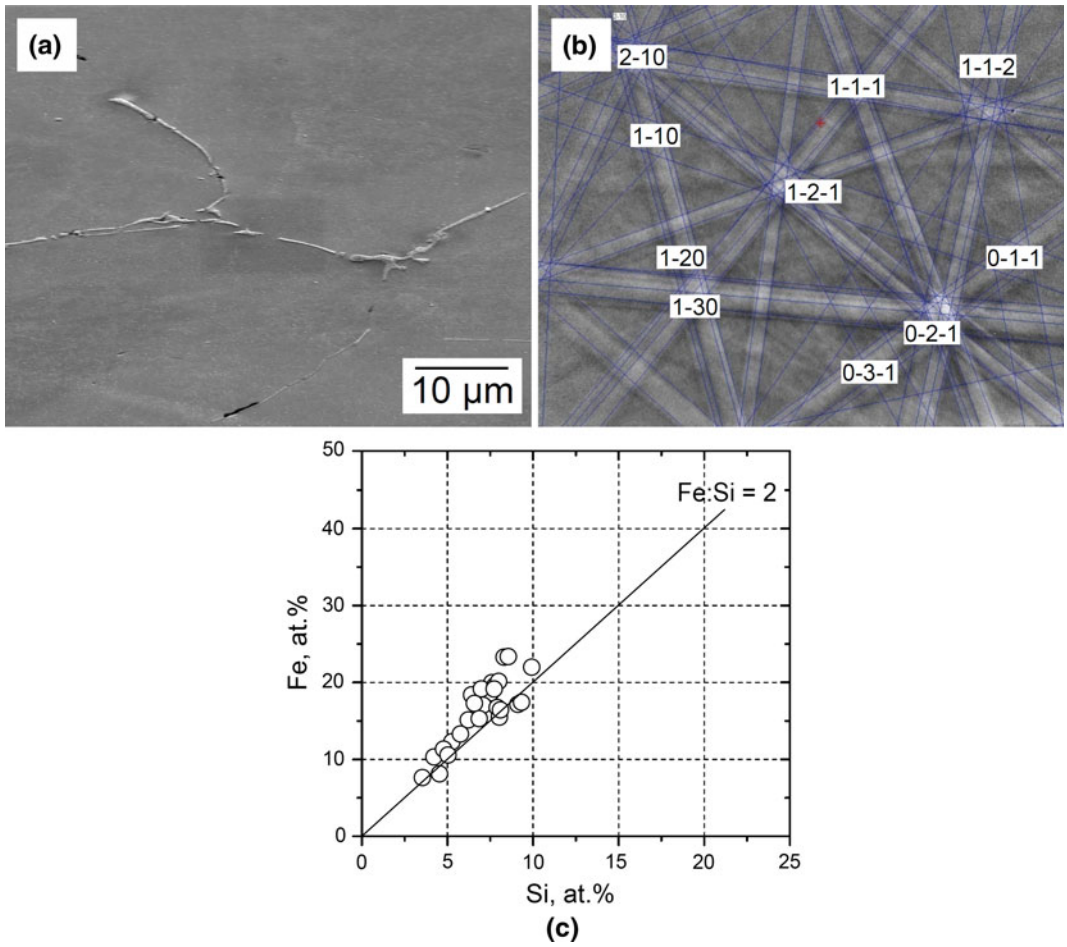

Fig. 7—(*a*) SEM SEI, (*b*) EBSD pattern, and (*c*) EDX analyses of Chinese-script intermetallic phase observed in the 6060 alloy containing 0.2 wt pct Fe. The EBSD pattern is indexed according to bcc α_c-AlFeSi.

bcc structure with a lattice parameter of 1.256 nm, indicating that the particles are not α_h-Al_8Fe_2Si, despite the ratios between Fe and Si (and Al) being close for this phase. Again, the intermetallic appears to be closest to the reported α_c-$Al_{19}Fe_4MnSi_2$. The fact that it is closer to $Al_{19}Fe_{4.4}Si_2$ seems to suggest that Mn has been substituted partially by Fe atoms and the remainder by vacancies. Diffraction patterns from the Al_3Fe are indexable according to a monoclinic crystal structure with $a = 1.549$ nm, $b = 0.808$ nm, $c = 1.248$ nm, and $\beta = 107.72$ deg.

F. *Phase Prediction Using THERMO-CALC*

The Scheil module of THERMO-CALC (version TCW4) coupled with TTAL4 aluminum alloy database was used to predict the phases formed during solidification of 6060 alloys with increasing Fe content. Temperature *vs* fraction solid curves are shown in Figures 11(a) and (b) for 0.1 and 0.5 wt pct Fe, respectively. These show that the identity of the Fe containing phases changes and the temperature at which they precipitate increases as the Fe content increases.

A graph of the predicted proportions of the various intermetallic phases as a function of Fe content is shown in Figure 11(c). THERMO-CALC predicts that as the Fe content increases, the amount of the initially-preferred Fe-containing phase increases, until another richer Fe-containing phase forms. At very low Fe contents (≤0.1 wt pct), THERMO-CALC predicts that mainly π-AlFeSi (*i.e.*, $Al_8FeMg_3Si_6$) and β-Al_5FeSi form. As the Fe content increases between 0.1 and 0.2 wt pct, there is a large increase in the predicted amount of α-AlFeSi (*i.e.*, α_h-Al_8Fe_2Si), while the amount of π-AlFeSi and β-AlFeSi remains constant. As the Fe content is increased above 0.2 wt pct, THERMO-CALC predicts that increasing amounts of Al_3Fe form, while the amounts of the other phases remain constant. Above 0.4 wt pct Fe, it is predicted that Al_3Fe is the dominant phase. In addition, as the Fe content increases, so does the temperature at which the first Fe-intermetallic is predicted to precipitate from the melt (Table III). At 0.1 to 0.2 wt pct Fe, α_h-Al_8Fe_2Si is predicted to be the first phase to precipitate, while at higher Fe contents, Al_3Fe forms before α_h-Al_8Fe_2Si (consistent with the phase observations seen in Figure 10(a)).

The Scheil module in THERMO-CALC does not take into account peritectic reactions/transformations that may occur during the solidification process. However,

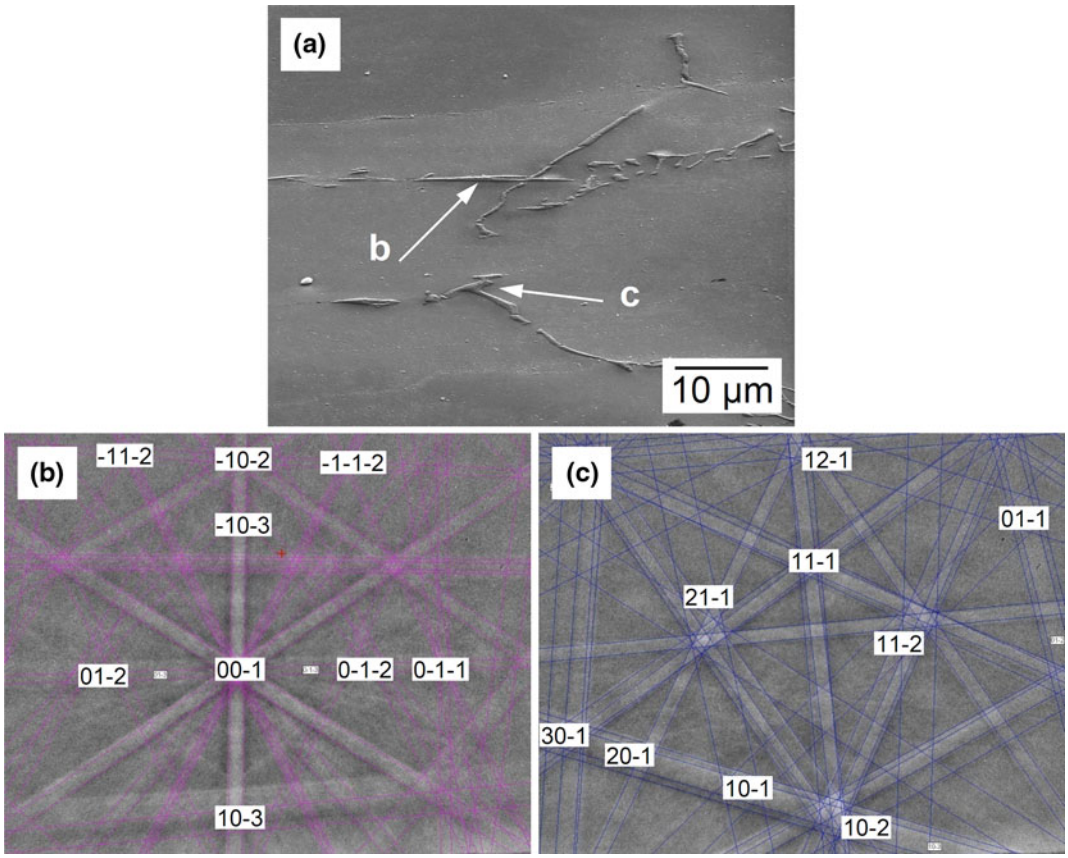

Fig. 8—(*a*) SEM SEI showing the presence of both α_c-AlFeSi (indicated "b") and Al_3Fe (indicated "c") in the 6060 alloy containing 0.5 wt pct Fe, (*b*) EBSD pattern of α_c-AlFeSi phase, and (*c*) EBSD pattern of Al_3Fe phase.

given phase equilibrium considerations, it could be expected that some of the Al_3Fe could transform to α_h-AlFeSi, which in turn could transform to β-Al_5FeSi. As stated earlier, this will be dependent upon nucleation and kinetic characteristics of these transformations.

IV. DISCUSSION

This study has shown how powerful it is to use a number of complementary microscopy and analytical techniques for phase characterization and identification. Optical microscopy is the simplest technique and provides an overview of the particle morphology and distribution but does not provide any chemical or crystallographic information. TEM is able to be used to determine the crystallography of the phases present, but provides very limited information on the distribution of the phases and might not be able to provide a representative sample of the alloy for solidified microstructures, which are inhomogeneous at the length scale at which TEM operates. The SEM with EDX is able to provide information of the fine-scale particle morphology and distribution of the phases as well as chemical information. However, in systems where there are phases with similar chemistries, such as the Al-Fe-Si phases here, crystallographic information is required to be confident that particles have been identified correctly. Moreover, although the method described by Qian *et al.*[34] is useful for distinguishing between α and β phases, the method is less practical for small particles, particularly when there is no Mn in the α phase to aid identification. Hence, the additional use of an EBSD detector provides a powerful phase identification technique. The use of TEM may still be required to characterize phase crystallography, but once this is known, phases can be identified rapidly and with great accuracy. In addition to these techniques, deep etching provides an insight into the 3-D intermetallic network structures.

A summary of the intermetallic observations made is given in Table IV. Two SEM microscopy techniques were found useful to distinguish between β and α phases. The first was the visual observation at high magnification in which the β phase was sometimes seen to have a lacy feature while the α phase was relatively featureless. This can be used as an indicator to distinguish β and α phases. Second, the use of EDX to give an indication of the Fe:Si ratio enables discrimination between β and α phases, with atomic ratios of approximately 1 and 2 to 2.5, respectively.[34] This method was found by Kuijpers *et al.*[35] to give a high accuracy estimate of the relative transformation of β to α during homogenization, with the absolute Mn concentration of individual intermetallic particles added to achieve a further slight error reduction. Nevertheless, since the Fe(+Mn):Si ratios

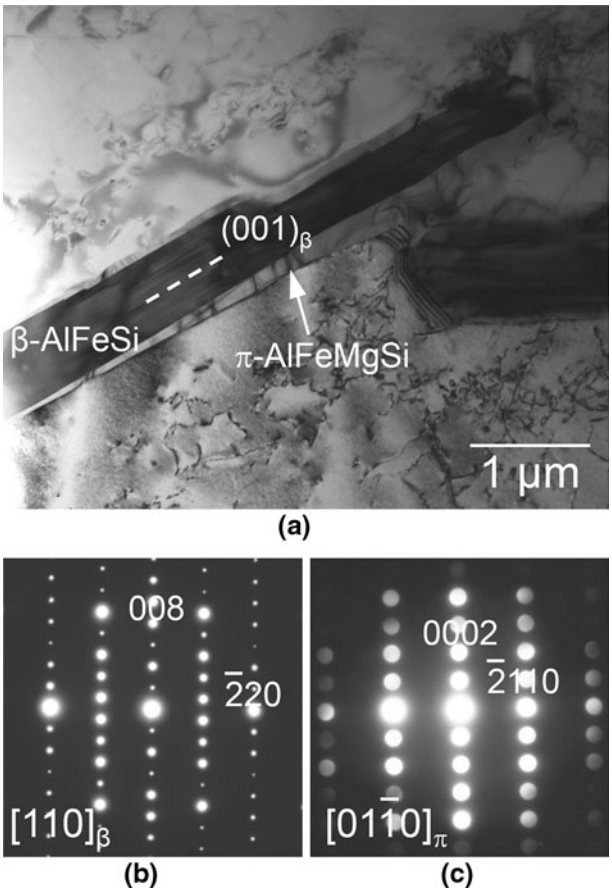

Fig. 9—(*a*) TEM image showing β-Al_5FeSi and π-$Al_8FeMg_3Si_6$ phases in the 6060 alloy with 0.3 wt pct Fe, (*b*) selected area electron diffraction pattern of β-Al_5FeSi, and (*c*) microbeam electron diffraction pattern of π-$Al_8FeMg_3Si_6$.

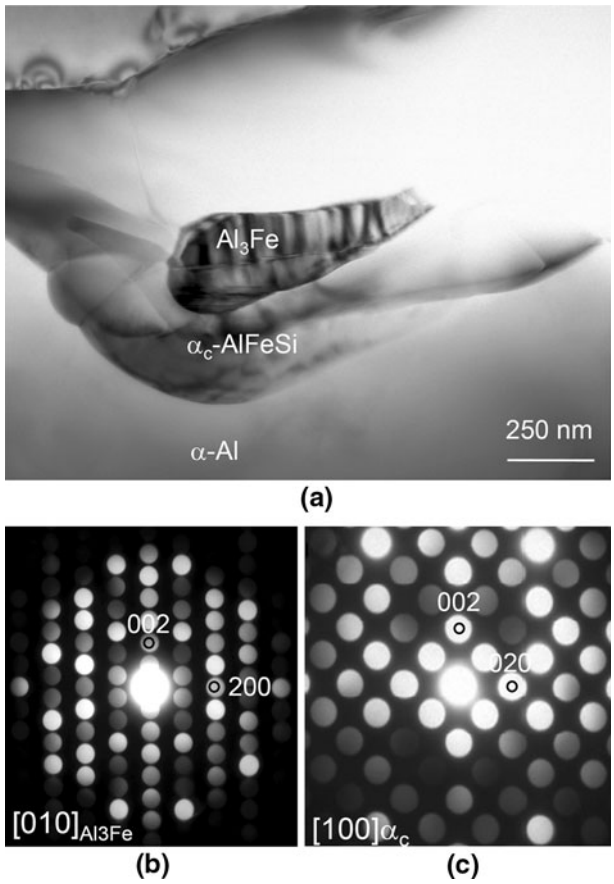

Fig. 10—(*a*) TEM image showing an Al_3Fe particle incorporated within α_c-AlFeSi phase in the 6060 alloy with 0.5 wt pct Fe, and corresponding selected area electron diffraction patterns of (*b*) the Al_3Fe phase and (*c*) the α_c-AlFeSi phase.

Table II. Comparison of Atomic Ratio of Al:Fe:Si in the α_c-AlFeSi Phase (as Measured Using EDX in the TEM) with the Reported Stoichiometries of Other Known α-AlFeSi Phases; the Three Particles Were All from the 0.5 Wt pct Fe Alloy

		α_h-	α_c-		
Particle	Measured Al:Fe:Si	Al_8Fe_2Si (8 : 2 : 1)	$Al_{12}Fe_3Si$ (12 : 3 : 1)	$Al_{15}(Fe,Mn)_3Si_2$ (15 : 3 : 2)	$Al_{19}Fe_4MnSi_2$ (19 : 4 : 2)
1	69.9:20.8:9.3	7.5:2.2:**1**	10.1:**3**:1.3	15.0:4.5:**2**	13.4:**4**:1.8
2	73.8:17.8:8.3	8.9:2.1:**1**	12.4:**3**:1.4	17.8:4.3:**2**	16.6:**4**:1.9
3	73.2:18.3:8.5	8.6:2.2:**1**	12.0:**3**:1.4	17.2:4.3:**2**	16.0:**4**:1.9

between the two α-AlFeSi phases (α_c and α_h) are similar and the morphologies are the same, it is still difficult to distinguish between the two α forms using EDX. Conversely, it was seen that the crystallographic information collected using SEM with EBSD is able to clearly distinguish between the two α forms.

It is generally assumed that the hexagonal form of the phase, α_h-Al_8Fe_2Si, is found in alloys with Mn < 0.01 wt pct[35,38–40] and that, once a small amount of Mn is added to the alloy, then the cubic form, α_c-$Al_{15}(Fe,Mn)_3Si_2$, is present instead.[12] It has also been observed that α_c-Al(Fe,Mn)Si can transform to α_h-Al(Fe,Mn)Si after homogenization.[28,39,41] Despite there being no Mn in the 6060 alloy (≤0.001 wt pct) used in this work, and for that matter no Mn being found in the intermetallic phase by EDX, it was evident using EBSD and TEM analyses that all of the α-AlFeSi phase present was cubic rather than hexagonal. In fact, no α_h-Al_8Fe_2Si was found in any of the alloys studied. Although the EDX results indicated that the Al:Fe:Si ratio was close to that of α_h (*i.e.*, 8:2:1, Table II), the best fit with the reported cubic α phases is with α_c-$Al_{19}Fe_4MnSi_2$[23] rather than α_c-$Al_{15}(Fe,Mn)_3Si_2$ or α_c-$Al_{12}Fe_3Si$.

The predominant phase in the microstructure up to 0.2 wt pct Fe was found to be the faceted β-Al_5FeSi

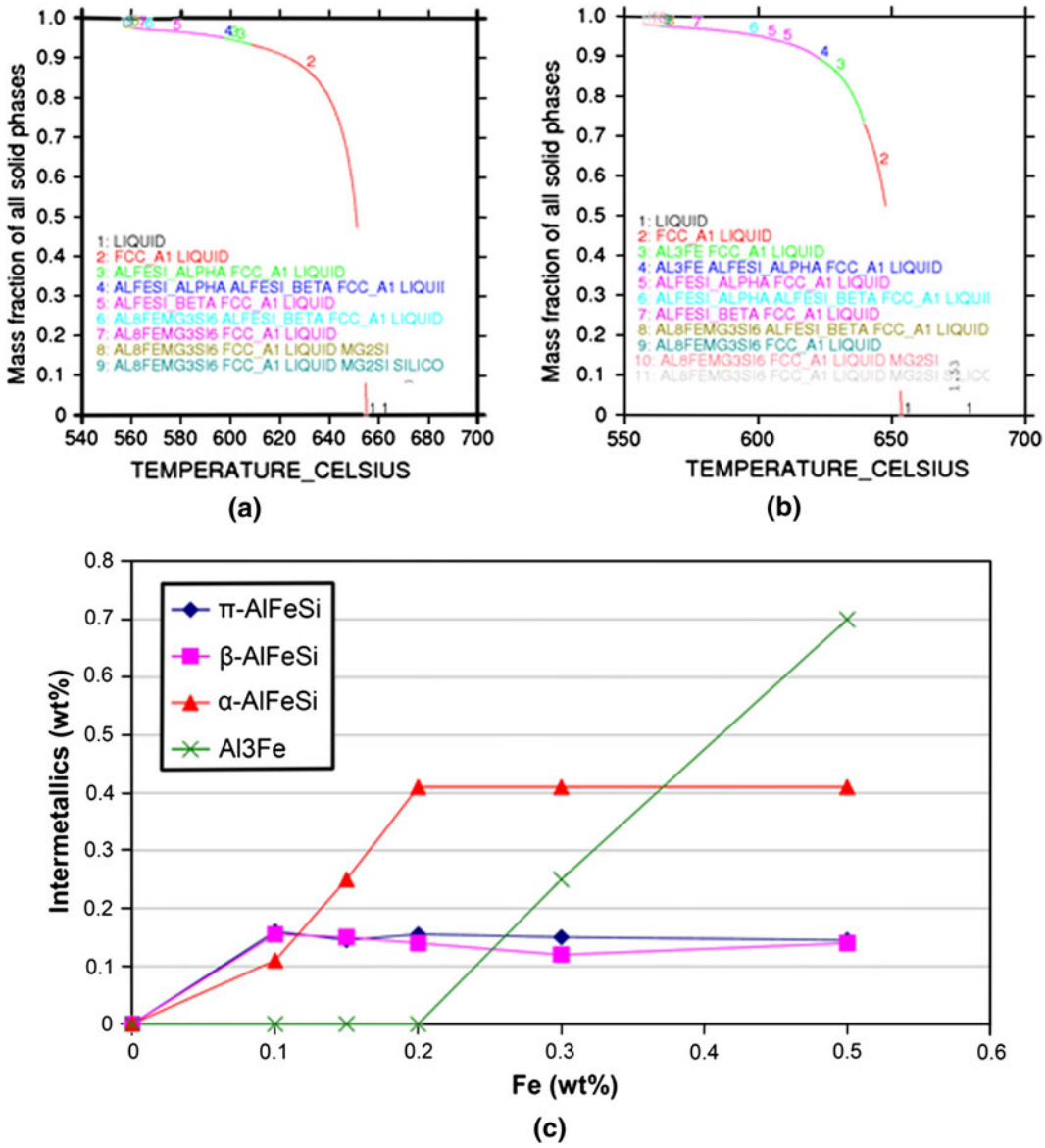

Fig. 11—Temperature *vs* fraction solid curves as predicted by THERMO-CALC assuming Scheil solidification and no peritectic reactions with (*a*) 0.1 pct Fe and (*b*) 0.5 wt pct Fe. (*c*) The amount of the Fe-containing intermetallic phases at the end of solidification, as predicted by THERMO-CALC. Note that α-AlFeSi in THERMO-CALC is equivalent to α_h-AlFeSi, β-AlFeSi to β-Al_5FeSi, and π-AlFeSi to π-$Al_8FeMg_3Si_6$.

Table III. Temperatures at Which the First Fe-Containing Phase Precipitates from the Melt According to THERMO-CALC for Alloy 6060

Fe (Wt pct)	Temperature [K (°C)]	Phase
0.1	881 (608)	α_h-AlFeSi
0.15	887 (614)	α_h-AlFeSi
0.2	896 (623)	α_h-AlFeSi
0.3	909 (636)	Al_3Fe
0.5	913 (640)	Al_3Fe

phase. At 0.2 wt pct Fe content, some Chinese-script morphology α_c-AlFeSi phase was observed and identified using EBSD in the SEM. Above 0.3 wt pct Fe, α_c-AlFeSi was the predominant phase, and at 0.5 wt pct Fe, no β-Al_5FeSi was observed. At 0.3 wt pct Fe, some Al_3Fe was also found, and the amount of this phase increased with an increase in the Fe content up to 0.5 wt pct. The predominance of β-Al_5FeSi at 0.2 wt pct Fe was observed by others,[42] and the identity of the phases at the higher Fe contents seems to agree reasonably well with previous work in a 6063 alloy.[28] In that work, however, Tanihata *et al.*[28,41] noted the presence of α_h-AlFeSi as well as β and α_c-AlFeSi in the as-cast condition, but no Al_3Fe was observed.

Apart from predicting the presence of α_h-AlFeSi rather than the α_c-AlFeSi form, the prediction of phase types from THERMO-CALC broadly agrees with the microstructural observations in this study. In terms of phase amounts, several discrepancies are evident. THERMO-CALC predicts that α_h-AlFeSi should be present at 0.1 wt pct Fe content, whereas neither form of α was verified microstructurally at this composition.

Table IV. Summary and Comparison of the Phases Identified in 6060 Alloy with Varying Nominal Fe Contents Using the Different Observation and Analytical Techniques

Fe (Wt pct)	Optical Observations	SEM (EBSD)	SEM (EDX)	TEM	THERMO-CALC
0.1	faceted phase (*i.e.*, elongated particles on grain boundaries)	β-Al_5FeSi	β Fe:Si $\approx$ 1	β-Al_5FeSi π-$Al_8FeMg_3Si_6$	β-Al_5FeSi α_h-AlFeSi π-$Al_8FeMg_3Si_6$
0.2	faceted phase (as above), plus some particles tending toward scriptlike	β-Al_5FeSi (major) α_c-AlFeSi (minor) π-$Al_8FeMg_3Si_6$ Al_3Fe (very small amount)	β Fe:Si $\approx$ 1 α Fe:Si $\approx$ 2	β-Al_5FeSi	β-Al_5FeSi α_h-AlFeSi (major) π-$Al_8FeMg_3Si_6$
0.3	faceted phase; some Chinese-script phase	β-Al_5FeSi α_c-AlFeSi Al_3Fe (minor)	β Fe:Si $\approx$ 1 α Fe:Si $\approx$ 2	β-Al_5FeSi π-$Al_8FeMg_3Si_6$	β-Al_5FeSi α_h-AlFeSi π-$Al_8FeMg_3Si_6$ Al_3Fe
0.5	Chinese-script phase predominantly	α_c-AlFeSi (major) Al_3Fe (minor)	α Fe:Si $\approx$ 2	α_c-AlFeSi Al_3Fe (minor)	β-Al_5FeSi α_h-AlFeSi π-$Al_8FeMg_3Si_6$ Al_3Fe

It also predicts that α is the dominant phase at 0.2 wt pct Fe rather than β-Al_5FeSi, as was actually observed. On the other hand, α_c-AlFeSi is the dominant phase observed at 0.5 wt pct Fe, while THERMO-CALC predicts it should be Al_3Fe. It is possible that a peritectic reaction has occurred where some of the Al_3Fe has been transformed to α_c-AlFeSi. As noted previously, peritectic reactions are not incorporated into the Scheil model of THERMO-CALC, and this may explain the discrepancy. Interestingly, a very small amount of Al_3Fe was found in the 0.2 wt pct Fe alloy, and THERMO-CALC also predicts that this is the composition at which it begins to form.

While the intermetallic α and β phases were the primary focus of the analyses of this study, it is worth noting that π-AlFeMgSi (*i.e.*, π-$Al_8FeMg_3Si_6$) was also observed in some alloys and only using TEM (Table IV), whereas THERMO-CALC suggested it should to be present in the microstructure of all the alloys. The reason for π-AlFeMgSi not being observed via SEM may be that it is less easily distinguished from the matrix in backscatter electron imaging due to the smaller atomic contrast, as it contains less Fe than the other Fe containing phases. Alternatively, it may form as a difficult-to-distinguish peritectic reaction product on the surface of the more dominant β-Al_5FeSi platelets (as observed in Figure 9(a)).

Deep etching revealed that what appeared optically to be discrete intermetallic phases, particularly at the lower Fe contents, are interconnected 3-D intermetallic structures. This shows, as indicated by Kuijpers,[43] that 2-D analyses can be misleading as they often give the impression of discrete particles when there is a highly connected 3-D structure. In the lower Fe content alloys, where β-Al_5FeSi was found to be the dominant phase present, an interconnected network of plates and needles was observed. While at 0.1 wt pct Fe, the network was not fully connected, at 0.2 wt pct Fe, it was. Increasing the Fe content further led to the formation of connected particles with a seaweed-like morphology consisting of petals and "dendrite" arms. It should be noted that this strongly networked 3-D intermetallic structure is in stark contrast to the discrete α_c-AlFeSi phase particles, which form during homogenization and exist as a string of small particles ($\approx$1 μm) located along the positions of the original β particles.[38]

V. CONCLUSIONS

The effects of Fe content on the formation of Fe-containing intermetallic phases in an as-cast AA6060 alloy have been examined using a range of microstructural characterization techniques – optical microscopy, SEM and TEM. It was found that this combination, when combined with EBSD and EDX in the SEM, was particularly powerful in the identification of phases with similar chemistry and composition, such as the Al-Fe-Si phases in 6xxx series alloys.

At Fe contents less than 0.2 wt pct, β-Al_5FeSi is the dominant Fe-containing phase with an Fe:Si ratio of approximately 1. At Fe contents around 0.2 wt pct, a 3-D connected network of intermetallic particles had developed. The α_c-AlFeSi phase was found to the exclusion of α_h-Al_8Fe_2Si and was predominant in the microstructure in alloys with 0.3 to 0.5 wt pct Fe. The Fe:Si ratio is close to 2 and fits more closely to the stoichiometry of α_c-$Al_{19}Fe_4MnSi_2$ than of α_c-$Al_{15}(Fe,Mn)_3Si_2$. A small amount of Al_3Fe was found in the microstructure at 0.3 wt pct Fe and this increased as the Fe content increased to 0.5 wt pct. The Al_3Fe phase was sometimes found to be rimmed by α_c-AlFeSi, indicating a peritectic reaction/transformation.

As Fe content in aluminum alloys increases, especially through increased recycling, understanding how these solidified microstructures transform at different Fe contents under subsequent processing operations will be key to optimizing the properties of these alloys.

ACKNOWLEDGMENTS

The CAST Cooperative Research Centre (CAST CRC) was established under and is supported, in part, by the Australian Government's Cooperative Research Centres Programme. The authors gratefully acknowledge the Monash Centre for Electron Microscopy (MCEM) for access to experimental facilities.

REFERENCES

1. S.K. Das: in *Light Metals 2006*, T.J. Galloway, ed., TMS, Warrendale, PA, 2006, pp. 911–16.
2. C.M. Dinnis, J.A. Taylor, and A.K. Dahle: *Mater. Sci. Eng. A*, 2006, vol. 425 (1–2), pp. 286–96.
3. C.M. Dinnis, J.A. Taylor, and A.K. Dahle: *Metall. Mater. Trans. A*, 2006, vol. 37A, pp. 3283–91.
4. E.D. Sweet, E.S. Charles, and M.J. Couper: *Mater. Forum*, 2004, vol. 28, pp. 1198–203.
5. S.F. Corbin, E. Ansah-Sam, and D.J. Lloyd: *Mater. Sci. Forum*, 2006, vols. 519–521, pp. 125–30.
6. J. Sarkar, T.R.G. Kutty, D.S. Wilkinson, J.D. Embury, and D.J. Lloyd: *Mater. Sci. Engng. A*, 2004, vol. 369 (1–2), pp. 258–66.
7. H. Nagaumi, S. Suzuki, T. Okane, and T. Umeda: *Mater. Trans.*, 2006, vol. 47 (11), pp. 2821–27.
8. A. Couture: *Int. Cast Met. J.*, 1981, vol. 6 (4), pp. 9–17.
9. P.N. Crepeau: *Trans. Am. Foundrymen's Soc.*, 1995, vol. 103, pp. 361–61.
10. T.O. Mbuya, B.O. Odera, and S.P. Ng'ang'a: *Int. J. Cast Met. Res.*, 2003, vol. 16 (5), pp. 451–65.
11. V. Stefániay, Á. Griger, and T. Turmezet: *J. Mater. Sci.*, 1987, vol. 22, pp. 539–46.
12. L.F. Mondolfo: *Aluminum Alloys: Structure and Properties*, Butterworths, Boston, MA, 1976.
13. G. Sha, K.A.Q. O'Reilly, B. Cantor, J.M. Titchmarsh, and R.G. Hamerton: *Acta Mater.*, 2003, vol. 51, pp. 1883–97.
14. J.N. Pratt and G.V. Raynor: *J. Inst. Met.*, 1951, vol. 79 (Part 4), pp. 211–32.
15. V.G. Rivlin and G.V. Raynor: *Int. Mater. Rev.*, 1981, vol. 26 (3), pp. 133–52.
16. R. Høier, O. Lohne, and S. Mørtvedt: *Scand. J. Metall.*, 1977, vol. 6 (1), pp. 36–37.
17. L. Bäckerud, E. Król, and J. Tamminen: *Solidification Characteristics of Aluminum Alloys Volume. 1: Wrought Alloys*, AFS/Skanaluminium, Oslo, Norway, 1993.
18. M.H. Mulazimoglu, A. Zaluska, J.E. Gruzleski, and F. Paray: *Metall. Mater. Trans. A*, 1996, vol. 27A, pp. 929–36.
19. G. Sha, K.A.Q. O'Reilly, and B. Cantor: *Mater. Sci. Forum*, 2006, vols. 519–521, pp. 1721–26.
20. M. Warmuzek, K. Rabczak, and J. Sieniawski: *J. Mater. Process. Technol.*, 2005, vols. 162–163, pp. 422–28.
21. M.V. Kral, H.R. McIntyre, and M.J. Smillie: *Scripta Mater.*, 2004, vol. 51 (3), pp. 215–19.
22. D. Munson: *J. Inst. Met.*, 1967, vol. 95, pp. 217–19.
23. P. Villers and L.D. Calvert: *Pearson's Handbook of Crystallographic Data for Intermetallic Phases*, 2nd ed., ASM INTERNATIONAL, Materials Park, OH, 1991, pp. 825–32.
24. M. Cooper: *Acta Crystallogr.*, 1967, vol. 23, pp. 1106–07.
25. D.J. Skinner, R.L. Bye, D. Raybould, and A.M. Brown: *Scripta Metall.*, 1986, vol. 20 (6), pp. 867–72.
26. S. Zajac, B. Hutchinson, A. Johansson, and L.O. Gullman: *Mater. Sci. Technol.*, 1994, vol. 10 (4), pp. 323–33.
27. C.Y. Sun and L.F. Mondolfo: *J. Inst. Met.*, 1967, vol. 95, p. 384.
28. H. Tanihata, T. Sugawara, K. Matsuda, and S. Ikeno: *J. Mater. Sci.*, 1999, vol. 34 (6), pp. 1205–10.
29. X. Doré, H. Combeau, and M. Rappaz: *Acta Mater.*, 2000, vol. 48 (15), pp. 3951–62.
30. F.H. Samuel, A.M. Samuel, H.W. Doty, and S. Valtierra: *Metall. Mater. Trans. A*, 2001, vol. 32A, pp. 2061–75.
31. M. Easton, H. Wang, J. Grandfield, D. StJohn, and E. Sweet: *Mater. Forum*, 2004, vol. 28, pp. 224–29.
32. S. Instone, D. StJohn, and J. Grandfield: *Int. J. Cast Met. Res.*, 2000, vol. 12 (6), pp. 441–56.
33. A.K. Gupta, P.H. Marois, and D.J. Lloyd: *Mater. Characterization*, 1996, vol. 37 (2–3), pp. 61–80.
34. M. Qian, J.A. Taylor, J.Y. Yao, M.J. Couper, and D.H. StJohn: *J. Light Met.*, 2001, vol. 1 (3), pp. 187–93.
35. N.C.W. Kuijpers, W.H. Kool, P.T.G. Koenis, K.E. Nilsen, I. Todd, and S. van der Zwaag: *Mater. Characterization*, 2003, vol. 49, pp. 409–20.
36. M.E. Glicksman and R.N. Hills: *Philos. Mag. A*, 2001, vol. 81 (1), pp. 153–59.
37. M.F. Zhu, C.P. Hong, D.M. Stefanescu, and Y.A. Chang: *Metall. Mater. Trans. B*, 2007, vol. 38B, pp. 517–24.
38. N.C.W. Kuijpers: *Kinetics of the β-AlFeSi to α-Al(FeMn)Si Transformation in AlMgSi Alloys*, Technische Universiteit Delft, Delft, 2004.
39. Y. Birol: *J. Mater. Process. Technol.*, 2004, vol. 148 (2), pp. 250–58.
40. N.C.W. Kuijpers, F.J. Vermolen, C. Vuik, P.T.G. Koenis, K.E. Nilsen, and S. van der Zwaag: *Mater. Sci. Eng. A*, 2005, vol. 394 (1–2), pp. 9–19.
41. H. Tanihata, K. Matsuda, and S. Ikeno: *J. Jpn. Inst. Light Met*, 1997, vol. 47 (10), pp. 515–20.
42. S. Ornurlu and A. Tekin: *J. Mater. Sci.*, 1994, vol. 29, pp. 1652–55.
43. N.C.W. Kuijpers, J. Tirel, D.N. Hanlon, and S. Van der Zwaag: *Mater. Characterization*, 2002, vol. 48 (5), pp. 379–92.